Journal of Solid State Chemistry **161,** 373–378 (2001)
doi:10.1006/jssc.2001.9345, available online at http://www.idealibrary.com on IDEAL®

Effect of Alkali Ions on the Amorphous to Crystalline Phase Transition of Silica

A. M. Venezia,*,[1] V. La Parola,† A. Longo,* and A. Martorana*,†

*ICTPN-CNR, via Ugo la Malfa 153, 90146 Palermo, Italy; and †Dipartimento di Chimica Inorganica, Università di Palermo, Viale delle Scienze, Palermo, Italy

Received May 2, 2001; in revised form July 30, 2001; accepted August 2, 2001

The effect of the addition of alkali ions to commercial amorphous silica, generally used as support for heterogeneous catalysts, has been investigated from the point of view of morphological and structural changes. Samples of alkali-doped silica were prepared by impregnation and subsequent calcination at various temperatures. The structural effect of Li, Na, K, and Cs was determined by use of techniques such as wide-angle (WAXS) and small-angle X-ray scattering (SAXS). The WAXS diffractograms, analyzed with the Rietveld method using the GSAS program, allowed qualitative and quantitative identification of the fraction of the different silica polymorphs like quartz, tridymite, and cristobalite. SAXS measurements, using the classical method based on Porod's law, yielded the total surface area of the systems. The calculated areas were compared with the surface areas determined by the nitrogen adsorption technique using the analytical method of Brunauer–Emmett–Teller. The results are explained in terms of sizes of the alkali ions and cell volume of the different crystalline phases. © 2001 Academic Press

Key Words: **amorphous silica; alkali ions; phase transition; WAXS; SAXS; BET.**

1. INTRODUCTION

Transition of amorphous silica to different crystalline phases, with consequent modification of the specific surface area and of bulk properties, like sizes and distribution of pores, has a relevant impact on the use of such material as support for heterogeneous catalysts. Amorphous silica has interesting features that make it a good support for catalysts (1, 2). It can be commercially found free of impurity and with very high surface area allowing for a high dispersion of the active component with no interaction with the support. The silica gel, as it shrinks, loses surface hydroxyls, forming a siloxane surface up to 1273 K before rearrangement to crystalline forms (1–4).

[1]To whom correspondence should be addressed. Fax: +39 091 6809399. E-mail: anna@ictpn.pa.cnr.it.

Depending on temperature and pressure, during crystallization, different silica minerals are formed. The most common species are quartz (density = 2.65 $g\,cm^{-3}$, cell volume = 113 $Å^3$, trigonal), tridymite (density = 2.27 $g\,cm^{-3}$, cell volume = 2110 $Å^3$, monoclinic), and cristobalite (density = 2.32 $g\,cm^{-3}$, cell volume = 171 $Å^3$, tetragonal) (3). These phases may form as type α, characterized by the above physical and structural properties, and type β, indicated as *low*-temperature and *high*-temperature phases, respectively. The β phases have higher symmetry and lower densities with respect to the α phases. The vitreous or amorphous silica is characterized by a density of 2.21 $g\,cm^{-3}$. At atmospheric pressure, quartz is stable up to 1143 K, tridymite is stable in the range 1143–1743 K, and cristobalite is stable in the range 1743–1973 K. All phase transformations are kinetically inhibited and for this reason are influenced by trace of impurities (5). Indeed, the introduction of additives, such as alkali metal ions, besides an intrinsic effect on the catalytic performance of the silica-supported catalysts (6–8), may have a determinant role in the attainment of a particular silica phase (2). The alkali ions would occupy interstitial sites, collapsing the Si–O–Si bridges and favoring the transition to crystalline species.

A detailed study of the effect of the different alkali ions on the surface area, porosity, and phase transition temperature of amorphous silica is here undertaken. The obtained information would be used in order to choose the most suitable alkali ion as additive to supports for specific catalytic purposes. The surface areas were determined from nitrogen adsorption isotherms using the Brunauer, Emmett, and Teller method (BET) and from SAXS measurements. The comparison between the two sets of data may yield information on the "open" porosity, accessible to nitrogen, and on the total porosity arising from all interfaces included clogged pores. Total porosity, although less important from the catalytic point of view, is quite relevant for the mechanical strength and stability of the material. The use of the WAXS diffraction technique allowed discriminating

0022-4596/01 $35.00

between different crystalline phases formed as functions of temperature, alkali species, and alkali loading.

2. EXPERIMENTAL

2.1. Sample Preparations

The alkali-doped silica samples were prepared by incipient wetness impregnation of silica (from Aldrich Chemical Co. with grain size between 45 and 75 μm, surface area of 546 m^2/g, and pore volume of 0.92 ml/g) with aqueous solution of alkali nitrates. The impregnation was carried out at room temperature for 24 h and with a fixed volume of the alkali solution of the appropriate concentration. In order to have a complete and uniform impregnation, the volume of the solution did not exceed the pore volume of silica. The amounts of added alkali ions are given in Table 1 as millimoles per gram of silica. The numbers 1 and 4 in the labels refer to samples with the low and the high alkali contents corresponding approximately to 0.4 and 2.0 mmol/g. The samples were calcined in air for 4 h at three different temperatures: 773 K, 1073 K, and 1273 K.

2.2. BET Analysis

The microstructural characterization was performed with a Carlo Erba Sorptomat 1900 instrument. The fully computerized analysis of the adsorption isotherm of nitrogen at liquid nitrogen temperature, allowed, through the BET approach, the specific surface area of the samples to be obtained. By analysis of the desorption curve, using the Dollimore and Heal calculation method, the pore size volume distribution was also obtained (9).

2.3. Structural Analysis

2.3.1. *SAXS.* Scattering data at small angles (SAXS) were collected with a Paar compact Kratky camera, equipped with step-scanning motor and a scintillator counter. A Philips PW 1830 X-ray generator produced the Cu $K\alpha$, Ni-filtered ($\lambda = 1.5418$ Å) incident beam. The SAXS curves were collected in the Q-range from 0.01 to 0.6 $Å^{-1}$ corresponding to lengths from 600 Å down to 10 Å. $Q = (4\pi/\lambda)\sin(\theta/2)$ is the momentum transfer where θ is the scattering angle and λ is the X-ray wavelength. On the basis of the scattering profile following the Porod law of the Q^{-3} decay, within a large interval of Q up to ~ 0.3 $Å^{-1}$, using slit-collimated beam (10), areas were obtained according to the previously adopted procedure (11, 12) based on Porod's approximation. The intercept from the linear part of the plot of the scattering intensity $J(Q) \times Q^3$ versus Q^3 gives the so-called Porod constant, P, which is related to the surface per unit volume, S/V, through the following equation,

$$S/V = \pi(P/K)\phi(1 - \phi),$$

with ϕ representing the volume fraction of the solid phase equal to the ratio of the bulk density d_b (0.6 g/cm^3 as determined experimentally for the pure silica, from accurate volume and weight determination) over the skeletal density, d_s (2.2 g/cm^3 (13)), K is the so-called "invariant" given by the integral of the SAXS intensity. The use of the invariant avoids scaling of the data in absolute electronic units.

2.3.2. *WAXS.* The WAXS measurements for the structure determination were carried out with a Philips vertical goniometer using Ni-filtered Cu $K\alpha$ radiation. A proportional counter and a 0.05° step size in 2θ were used. The relative percentage of the crystalline phases present in each sample was obtained with the Rietveld refinement procedure (14). Pseudo-Voight functions with peak asymmetry correction were used for the simulation of the peak shapes (15). The calculations were performed with the program package GSAS (16).

TABLE 1
Alkali Ion (M^+) Content of the Silica Samples

Sample	M^+ (mmol/g)
SiO_2	0
1Li /SiO_2	0.37
1Na/SiO_2	0.44
1K/SiO_2	0.37
1Cs/SiO_2	0.42
4Li/SiO_2	2.0
4Na/SiO_2	1.9
4K/SiO_2	2.0
4Cs/SiO_2	1.9

3. RESULTS

The pore size range derived from desorption isotherms, and the surface areas obtained from BET and SAXS measurements, are reported in Tables 2 and 3 for the samples calcined at 773 K and 1073 K, respectively. The decrease of the surface area of amorphous silica is related to the type of alkali ion and to the calcination temperature. Upon air treatment at 1273 K, the areas for high alkali concentration decrease below the detection limit of the BET techniques. The SAXS profiles in logarithm scales are shown in Fig. 1 for pure silica and for 0.4 mmol/g sodium-doped silica, treated at different temperatures. Similar curves are obtained for the other samples.

In Fig. 2 the correlation between SAXS-derived areas and BET-derived areas is given. The experimental error on the BET-derived area is usually estimated around 10% of the values (9) where the estimated error for the SAXS derived area is of the order of 20% arising from errors in the bulk and skeletal density determination. Most of the differences between the two sets of data are within the experimental

TABLE 2
Specific Surface Area (m^2/g) As Obtained from BET and SAXS Analyses for the Supports Calcined at 773 K[a]

Sample	Pore size (Å)	S_{BET} (± 10%)	S_{SAXS} (± 20%)
SiO_2	20–40	550	400
1Li /SiO_2	10–50	500	370
1Na/SiO_2	30–65	197	159
1K/SiO_2	10–50	270	157
1Cs/SiO_2	30–50	221	188
4Li/SiO_2	30–200	213	147
4Na/SiO_2	200–300	13	36
4K/SiO_2	30–65	172	90
4Cs/SiO_2	80–200	41	67

[a]The pore sizes from nitrogen physisorption measurements are also reported. The errors on the surface area values are given in parentheses.

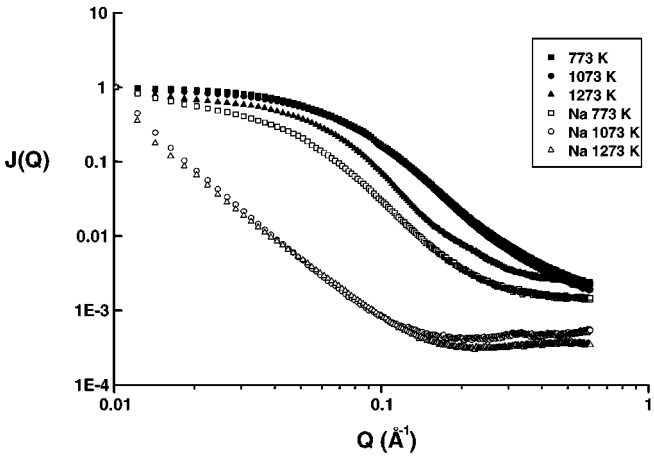

FIG. 1. Small-angle X-ray scattering profile of pure silica (solid symbols) and 1Na/SiO_2 (open symbols) after thermal treatments.

errors; however, the SAXS values are generally smaller than the BET ones.

The WAXS diffractograms relative to Li-, Na-, K-, and Cs-doped silica, calcined at different temperatures, are shown in Figs 3–6. The most intense reflections due to different crystalline phases are labeled in each diffractogram. The diffractograms of Fig. 3 referring to the lithium-doped silica indicate that the sample is still completely amorphous after calcination at 773 K (3a); it contains quartz after calcination at 1073 K (3b) and both quartz and cristobalite after treatment at 1273 K (3c). The difference between the low- and high-concentration lithium-doped samples consisted of the formation of lithium silicate in the latter sample. Concerning the sodium-doped silica, only transition to cristobalite was observed. The temperature of the transition is inversely dependent on the amount of the added species. For the largest size ions, potassium and cesium, the amorphous to crystalline transition is observed only in the high alkali ion concentration samples. As shown in Fig. 5 for the potassium-doped silica, the amorphous phase transforms to tridymite and cristobalite at 1073 K (Fig. 5b) with further crystallization to trydimite after calcination at 1273 K (Fig. 5c). The diffractograms of the cesium-doped silica, shown in Fig. 6, indicate similar behavior except for a poorer capacity of the cesium ion to promote the crystallization. Cesium nitrate, used as precursor, is still present in the 773 K calcined sample (Fig. 6a), and it is burned off at higher temperatures.

The percentages of each crystalline phase, as estimated by the Rietveld analyses of selected diffractograms, are listed in Table 4. Based on the assumption that the crystalline and amorphous phases have the same chemical composition and therefore equal scattering factors, the relative percentage of the amorphous phase could be estimated by nonlinear least-square fitting of the raw data. The relative percentage of the amorphous phase with respect to the crystalline phase was calculated from the ratio of the amorphous peak area over the sum of the areas of crystalline and amorphous peaks. The obtained values are given also in Table 4. As an example of the Rietveld approach, the refined and the observed profiles for the potassium- and cesium-doped silica are shown in Fig. 7. The low-temperature phases, α tridymite and α cristobalite (17), were used as input structures for the fitting procedure of these diffractograms. The interval of 2θ between 20 and 25, is shown in more detail in

TABLE 3
Specific Surface Area As Obtained from BET and SAXS Analyses of the Samples Calcined at 1073 K[a]

Sample	Pore size (Å)	S_{BET} (± 10%)	S_{SAXS} (± 20%)
SiO_2	10–40	547	416
1Li /SiO_2	40–100	44	55
1Na/SiO_2	200–300	0.2	0.6
1K/SiO_2	100–200	8	0.8
1Cs/SiO_2	200–300	0	29
4Li/SiO_2	100–300	33	n.d.
4Cs/SiO_2	200–300	3	n.d.

[a]The pore sizes from nitrogen physisorption measurements are also reported.

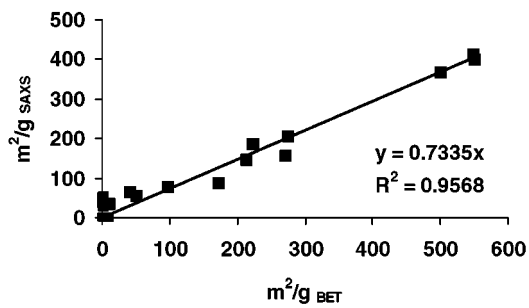

FIG. 2. Correlation between SAXS- and BET-derived surface areas.

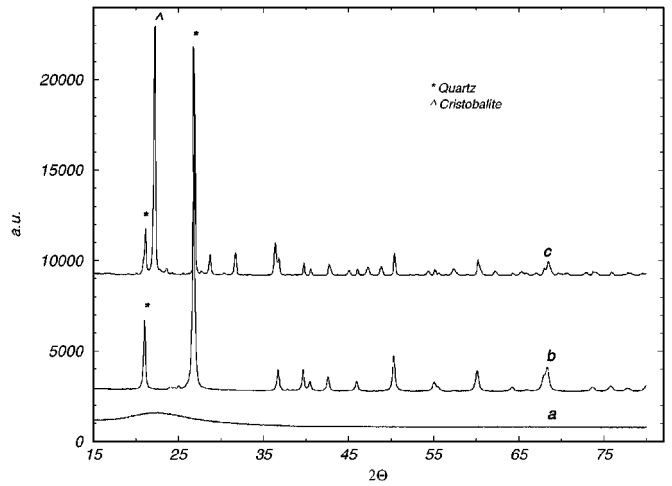

FIG. 3. XRD patterns of $1Li/SiO_2$ calcined at (a) 773 K, (b) 1073 K, and (c) 1273 K.

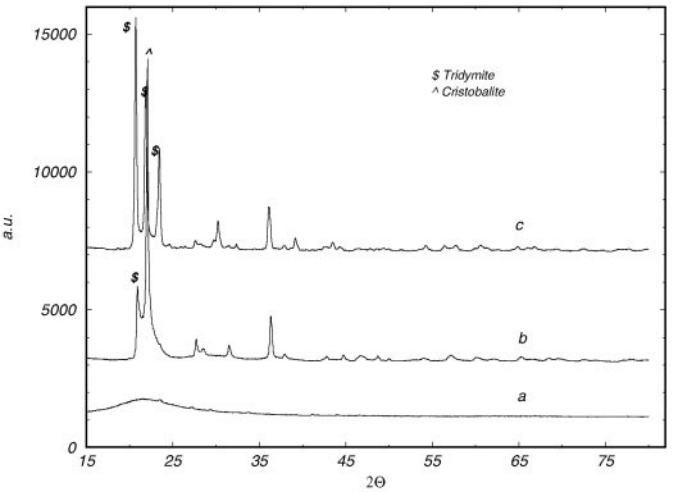

FIG. 5. XRD patterns of $4K/SiO_2$ calcined at (a) 773 K, (b) 1073 K, and (c) 1273 K.

the left panel of the figure. The corresponding unit cell parameters and the statistical factors obtained from the refinement procedure are listed in Table 5. Variations in the cell parameters cannot be considered significant; they probably arise from the fitting procedure applied to a small number of good quality peaks.

4. DISCUSSION

The scattering curves, displayed in Fig. 1, for the pure silica and for the sodium-doped samples are indicative of polydisperse systems with differences in pore dimension (18). Shifting of the slope to larger Q is generally indicative of smaller pore sizes (19). Accordingly, the scattering curves of the sodium-doped samples indicate formation of larger pores already at 773 K, in agreement with the diminished surface area. Analogous behavior is exhibited by the other alkali-doped samples.

As indicated in Fig. 2, the SAXS-derived values are generally smaller than the BET data. This type of trend has already been observed in some leached borosilicate glasses (13). The differences between the two sets of values were ascribed to the capability of the BET method to probe length scales comparable to the size of the nitrogen molecule (about 2 Å). In contrast, SAXS analysis, within the Porod approximation, probes length scales larger than 20 Å. An additional reason for the observed discrepancies between SAXS and BET area values is the presence of clogged porosity which, being seen by the SAXS technique but not

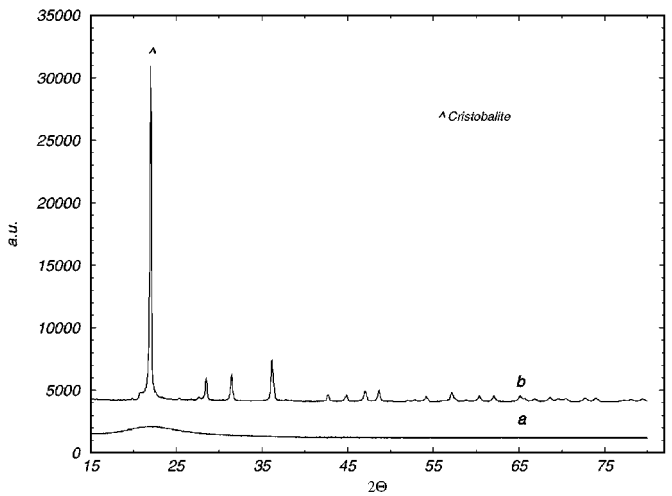

FIG. 4. XRD patterns of $1Na/SiO_2$ calcined at (a) 773 K and (b) 1073 K.

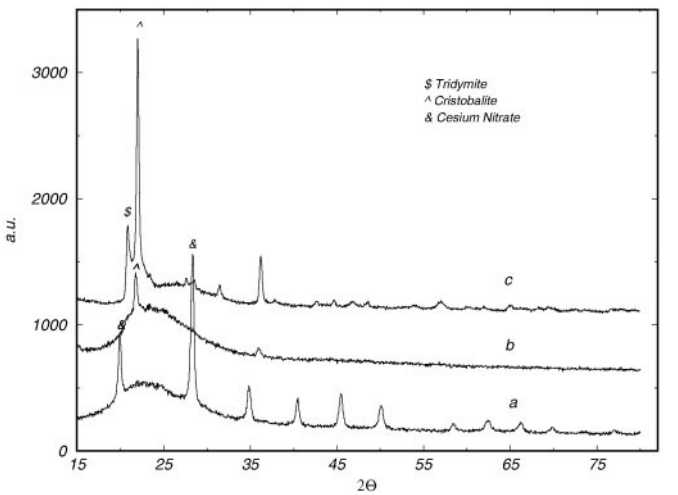

FIG. 6. XRD patterns of $4Cs/SiO_2$ calcined at (a) 773 K, (b) 1073 K, and (c) 1273 K.

TABLE 4
Percentage of Crystalline Phases[a] and of Amorphous Phase[b] for Samples Calcined at Two Different Temperatures[c]

Sample	T_c (K)	% $LiSi_2O_5$	% Quarz	% Tridymite	% Cristobalite	% Amorphous
$4Li/SiO_2$	1073	32	68	—	—	0
$1Li/SiO_2$	1273	—	43	—	57	0
$1Na/SiO_2$	1073	—	—	—	100	0
$4K/SiO_2$	1073	—	—	50	35	15
$4K/SiO_2$	1273	—	—	79	16	5
$4Cs/SiO_2$	1273	—	—	42	35	23

[a]Obtained from the Rietveld refinement procedure.
[b]From a nonlinear least-squares fitting of the raw data.
[c]The percentage error on the reported values is $\pm$ 5%.

TABLE 5
Unit Cell Data for Tridymite and Cristobalite and Reliability Factors Obtained from Rietveld Analysis of the Diffractograms of Potassium and Cesium Calcined at Different Temperatures

	$4K/SiO_2$, 1073 K	$4K/SiO_2$, 1273 K	$4Cs/SiO_2$, 1273K
Crystal system (tridymite)	Monoclinic	Monoclinic	Monoclinic
Space group	*C*1*C*1	*C*1*C*1	*C*1*C*1
a (Å)	18.318(5)	18.410(4)	18.371(6)
b (Å)	5.024(1)	4.986(1)	5.047(2)
c (Å)	26.009(5)	25.873(5)	26.106(6)
β	117.8(2)	117.8(2)	117.8(2)
Crystal system (cristobalite)	Tetragonal	Tetragonal	Tetragonal
Space group	$P4_12_12$	$P4_12_12$	$P4_12_12$
a (Å)	4.957(1)	4.953(6)	4.974(1)
b (Å)	4.957(1)	4.953(6)	4.974(1)
c (Å)	6.956(1)	6.957(9)	6.978(2)
*R*p (%)	5.2	3.6	3.9
*R*wp (%)	6.3	5.4	5.0
χ^2	2.28	1.51	0.52

Note. Calculated standard deviations in parentheses. $Rp = 100(\sum|I_o - I_c|/\sum I_o)$, $Rwp = 100(\sum w(I_o - I_c)^2/\sum wI_o^2)^{-1/2}$ according to Ref. (14).

by the BET adsorption method, may yield larger SAXS-derived areas. However, this is not the case here and therefore nothing can be said about the presence of such type of porosity. It is important to notice, from inspection of Tables 1, 2 and 3, how the addition of the alkali ions produces a substantial decrease of the surface area. The effect is enhanced by the increase of alkali concentration and of calcination temperature, driving the transition from amorphous to crystalline phases.

As the diffractograms of Figs. 3–6 indicate, the transition from amorphous silica to different crystalline phases depends on the type of doping ion. In particular, a certain relation between the size of the ion and the cell volume of the crystalline phase exists. Small ions like lithium, characterized by the ionic radius of 0.59 Å, induce transition to quartz at 1073 K in accord with previous findings (2). An increase in temperature produces a further transformation to cristobalite. Sodium (ionic radius of 0.99 Å) favors the transition to cristobalite in agreement with other studies (2, 20). Both potassium (ionic radius of 1.37 Å) and cesium (ionic radius of 1.67 Å) exhibit structural effects when present in large amount (2 mmol/g), determining the phase transition from amorphous to tridymite and cristobalite.

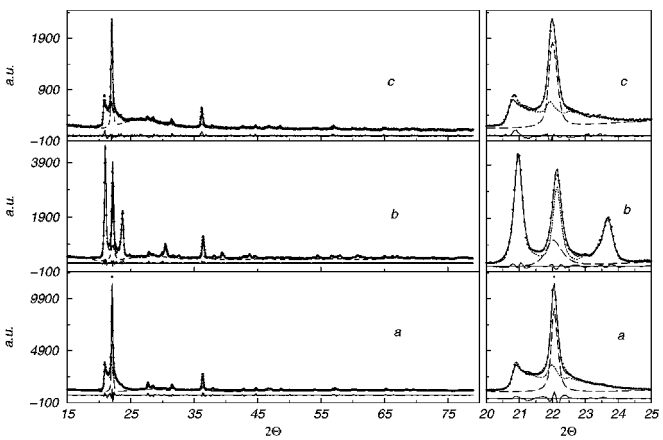

FIG. 7. Observed (circles) and calculated (continuous line) profiles of (a) $4K/SiO_2$ sample after calcination at 1073 K, (b) $4K/SiO_2$ sample after calcination at 1273 K, and (c) $4Cs/SiO_2$ sample after calcination at 1273 K. The curves underneath the diffractograms represent the difference between the profiles. The left panel shows the magnified 2θ interval from 20 to 25. The dotted line refers to the tridymite phase and the dashed line refers to the cristobalite phase.

Molecular orbital calculation (21) of thermodynamic and structural properties of pure and alkali-doped silica had indicated negligible changes of the SiO bond distance for crystalline, molten, and glassy states. In contrast, the SiOSi angles exhibited large variations, accounting probably for the polymorphism of the crystalline silica. According to the MO calculations, nonframework ions of smallest size and largest charge have the largest perturbation effect; therefore, Li > Na > K > Cs (21). Indeed, lithium and sodium are able to lower to 1073 K the transition temperature of amorphous to crystalline phase even when present in a small amount, about 0.4 mmol/g. In contrast, larger concentrations of K and Cs are needed to induce the transition at the same temperature. According to the experimental diffractograms and to the Rietveld refinement results, the effect of the temperature on the phase transition does not follow exactly the thermodynamic stability order of the pure silica phases. Moreover, the destabilization of the amorphous state with respect to the different crystalline phases

seems to be related to the size of the particular ion and how it compares with the size of the cell of the silica polymorphs. The reason for such behavior could be the possibility of the dopant ion to enter into the crystalline structure and act as nucleation center of a particular crystal phase. Small lithium ions are not able to stabilize the large tridymite cell whereas the larger ions like Na, K, and Cs are not able to stabilize the small quartz cell. Among the considered ions, sodium acts as the greatest destabilizer of amorphous silica, it induces the transition to cristobalite at a lower temperature as compared to the other ions, with a consequently drastic reduction of the surface area. The direct transition to cristobalite phase could be attributed to the size of the sodium ion, too large to be accommodated in the quartz structure, and too small to have any effect on the nucleation of the tridymite cell. In the perspective of using alkali-promoted silica as support for heterogeneous catalysts, besides electronic or geometric effects (7), structural modification induced by different ions should be taken into consideration.

5. CONCLUSION

The effect of alkali ions on amorphous silica can be considered from the point of view of solid state reaction. In other words, calcination at high temperature of amorphous silica, impregnated with alkali ion solutions, determines a reaction between the amorphous silica and the alkali oxide which, dependent on the physical characteristics of the ion, such as size and charge, drives the transition to the different crystalline phases of silica. The effect of the temperature on the transition from one phase to another generally should follow the thermodynamic stability order of the pure phases. However, depending on the mismatch between the ion size and the crystalline cell size, transition to some of the polymorphs does not occur. Therefore, the structural modification and the consequent reduction of the surface area should be first considered in making the choice of a particular alkali ion as a promoter of silica, used as support in heterogeneous catalysis.

ACKNOWLEDGMENT

The authors acknowledge the financial support from Progetto Finalizzato M.S.T.A. II.

REFERENCES

1. R. Voyatzis and J. B. Moffat, *J. Catal.* **142,** 45 (1993).
2. M. P. Mc Daniel, D. R. Witt, and E. A. Benham, *J. Catal.* **176,** 344 (1998).
3. R. K. Iler, "Chemistry of Silica." Wiley, New York, 1979.
4. F. A. Cotton, G. Wilkinson, C. A. Murillo, and M. Bochmann, "Advanced Inorganic Chemistry," 6th Ed., Wiley, New York, 1999.
5. A. Feltz, "Amorphous Inorganic Materials and Glasses." VCH, Weinheim, 1993.
6. A. M. Venezia, F. Raimondi, V. La Parola, and G. Deganello, *J. Catal.* **194,** 393 (2000).
7. A. M. Venezia, A. Rossi, L. F. Liotta, A. Martorana, and G. Deganello, *Appl. Catal. A* **147,** 81 (1996).
8. A. Palermo, J. P. Holgado Vazquez, A. F. Lee, M. S. Tikhov, and R. M. Lambert, *J. Catal.* **177,** 259 (1998).
9. S. J. Gregg and K. S. Sing, "Adsorption, Surface Area and porosity," 2nd Ed. Academic Press, San Diego, 1982.
10. G. Porod, *in* "Small-Angle X-ray Scattering" (H. Brumberger, Ed.). Gordon and Breach, New York, 1965.
11. J. Goodisman, H. Brumburger, and R. Cupelo, *J. Appl. Crystallogr.* **14,** 305 (1981).
12. G. Deganello, L. F. Liotta, A. Longo, A. Martorana, Y. Yanev, and N. Zotov, *J. Non-Cryst. Solids* **232,** 547 (1998).
13. D. W. Schaefer, R. K. Brow, B. J. Olivier, T. Rieker, G. Beaucage, L. Hrubesh, and J. S. Lin, *in* "Modern Aspect of Small-Angle Scattering" (H. Brumberger, Ed.), pp. 299–307. Kluwer, Dordrecht, 1995.
14. H. M. Rietveld, *J. Appl. Crystallogr.* **2,** 65 (1969).
15. L. Finger, D. E. Cox, and A. P. Jephcoat, *J. Appl. Crystallogr.* **27,** 892 (1994).
16. C. Larson and R. B. Von Dreele, Report LAUR 86-748, Los Alamos Laboratory, Los Alamos, NM, 1988.
17. K. K. Nukuiya, *Acta Crystallogr. B* **24,** 1968 (1982).
18. P. Fratzl, G. Vogl, and S. Klaumunzer, *J. Appl. Crystallogr.* **24,** 588 (1991).
19. A. Guinier and G. Fournet, "Small Angle Scattering of X-Rays." Wiley, New York and Chapman and Hall, London, 1955.
20. H. Zhang, J.-z Niu, Y. Kou, T. Tanaka, and S. Yoshida, *J. Cryst. Solid State* **137,** 325 (1998).
21. A. Navrotsky, K. L. Geisinger, P. McMillan, and G. V. Gibbs, *Phys. Chem. Miner.* **11,** 284 (1985).